Raman Spectrum of Graphene and Graphene Layers

A. C. Ferrari,[1,*] J. C. Meyer,[2] V. Scardaci,[1] C. Casiraghi,[1] M. Lazzeri,[3] F. Mauri,[3] S. Piscanec,[1] D. Jiang,[4] K. S. Novoselov,[4] S. Roth,[2] and A. K. Geim[4]

[1]*Cambridge University, Engineering Department, JJ Thompson Avenue, Cambridge CB3 0FA, United Kingdom*
[2]*Max Planck Institute for Solid State Research, Stuttgart 70569, Germany*
[3]*IMPMC, Universités Paris 6 et 7, CNRS, IPGP, 140 rue de Lourmel, 75015 Paris, France*
[4]*Department of Physics and Astronomy, University of Manchester, Manchester, M13 9PL, United Kingdom*

(Received 9 June 2006; published 30 October 2006)

Graphene is the two-dimensional building block for carbon allotropes of every other dimensionality. We show that its electronic structure is captured in its Raman spectrum that clearly evolves with the number of layers. The *D* peak second order changes in shape, width, and position for an increasing number of layers, reflecting the change in the electron bands via a double resonant Raman process. The *G* peak slightly down-shifts. This allows unambiguous, high-throughput, nondestructive identification of graphene layers, which is critically lacking in this emerging research area.

DOI: 10.1103/PhysRevLett.97.187401 PACS numbers: 78.67.Bf, 63.20.Dj, 63.20.Kr, 78.30.−j

The current interest in graphene can be attributed to three main reasons. First, its electron transport is described by the Dirac equation and this allows access to quantum electrodynamics in a simple condensed matter experiment [1–5]. Second, the scalability of graphene devices to nanodimensions [6–10] makes it a promising candidate for applications, because of its ballistic transport at room temperature combined with chemical and mechanical stability. Remarkable properties extend to bilayer and few-layers graphene [4–6,8,11]. Third, various forms of graphite, nanotubes, buckyballs, and others can all be viewed as derivatives of graphene and, not surprisingly, this basic material has been intensively investigated theoretically for the past 60 years [12]. The recent discovery of graphene [1] at last allows us to probe it experimentally, which paves the way to better understanding the other allotropes and to resolve controversies.

Graphene can be obtained using the procedure of Ref. [1], i.e., micromechanical cleavage of graphite. Alternative procedures, such as exfoliation and growth, so far only produced multilayers [6,8,13], but it is hoped that in the near future efficient growth methods will be developed, as happened for nanotubes. Despite the wide use of the micromechanical cleavage, the identification and counting of graphene layers is a major hurdle. Monolayers are a great minority amongst accompanying thicker flakes. They cannot be seen in an optical microscope on most substrates. They only become visible when deposited on oxidized Si substrates with a finely tuned thickness of the oxide layer (typically, 300 nm SiO_2) since, in this case, even a monolayer adds to the optical path of reflected light to change the interference color with respect to the empty substrate [1,4]. Atomic force microscopy (AFM) has been so far the only method to identify single and few layers, but it is low throughput. Moreover, due to the chemical contrast between graphene and the substrate (which results in an apparent chemical thickness of 0.5–1 nm, much bigger of what expected from the interlayer graphite spacing [1,4]), in practice, it is only possible to distinguish between one and two layers by AFM if films contain folds or wrinkles [1,4]. This poses a major limitation to the range of substrates and is a setback for the widespread utilization of this material. Here, we show that graphene's electronic structure is uniquely captured in its Raman spectrum. Raman fingerprints for single layers, bilayers, and few layers reflect changes in the electron bands and allow unambiguous, high-throughput, nondestructive identification of graphene layers, which is critically lacking in this emerging research area.

Here the samples are prepared by micromechanical cleavage [1]. To provide the most definitive identification of single and bilayers (beyond the AFM counting procedure) we perform transmission electron microscopy (TEM) on some of the samples to be measured by Raman spectroscopy. Samples for TEM are prepared following a similar process to that previously used to make freestanding and TEM-compatible nanotube devices [14]. In addition, this allows us to have freestanding layers on a grid easily seen in an optical microscope, facilitating their location during Raman measurements, Fig. 1(a). Electron diffraction is done in a Zeiss 912 Ω microscope at a voltage of 60 kV, and high-resolution images are obtained with a Philips CM200 microscope at 120 kV. A high resolution-TEM analysis of foldings at the edges or within the free-hanging sheets gives the number of layers by direct visualization, since at a folding the sheet is locally parallel to the beam, Figs. 1(b)–1(e). Edges and foldings of one or two layers are dominated by one or two dark lines, respectively. The number of layers is also obtained by a diffraction analysis of the freely suspended sheets for varying incidence angles, and confirms the number of layers from the foldings, Figs. 1(d) and 1(e). In particular, the diffraction analysis of the bilayer shows that it is *A*-*B* stacked (the intensity of the 11–20 diffraction spots (outer hexagon) is roughly twice that of the 1–100 (inner hexagon), Fig. 1(h), in agreement with diffraction simulations obtained by a

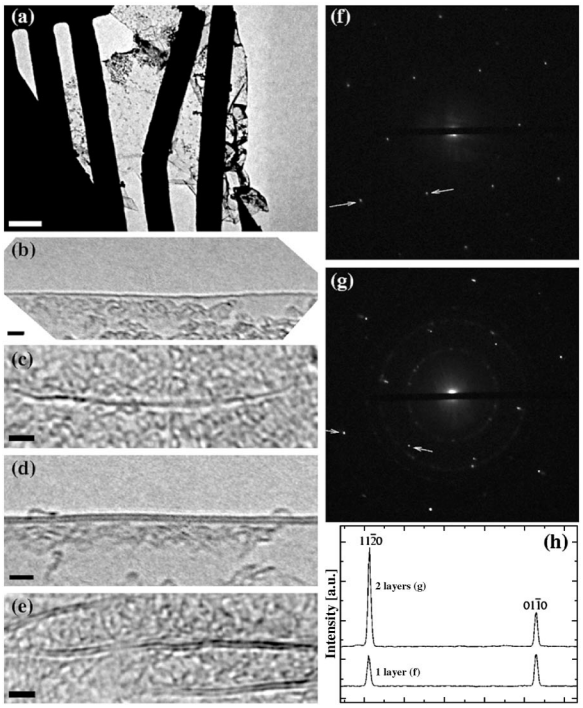

FIG. 1. (a) TEM of suspended graphene. The grid is also visible in optical microscopy. (b) High-resolution image of a folded edge of a single layer and (c) a wrinkle within the layer. (d) Folded edge of a two layer, and (e) internal foldings of the two layer. The amorphous contrast on the sheets is most likely due to hydrocarbon adsorbates on the samples that were cracked by the electron beam. (f) Electron diffraction pattern for close to normal incidence from single layer and (g) from two layers. Weak diffraction peaks from the supporting metal structure are also present. (h) Intensity profile plot along the line indicated by the arrows in (f),(g). The relative intensities of the spots in the two layer are consistent only with *A*-*B* (and not *A*-*A*) stacking. Scale bars: (a) 500 nm; (b–e) 2 nm.

Fourier transform of projected atomic potentials. This confirms our multilayer graphene has the same stacking as graphite.

Raman spectra are measured on single, bi, and multilayers on Si + SiO_2. Some are then processed into free-hanging sheets, as described above, and measured again after TEM. The measurements are performed at room temperature with a Renishaw spectrometer at 514 and 633 nm, with notch filters cutting at $\sim 100\ \mathrm{cm}^{-1}$. A 100× objective is used. Extreme care is taken to avoid sample damage or laser induced heating. Measurements are performed from ~4 to ~0.04 mW incident power. No significant spectral change is observed in this range. The Raman spectra of suspended and on-substrate graphene are similar, the main difference being a small *D* peak in the TEM samples. We also measure the reference bulk graphite used to produce the layers.

Figure 2(a) compares the 514 nm Raman spectra of graphene and bulk graphite. The two most intense features are the *G* peak at $\sim 1580\ \mathrm{cm}^{-1}$ and a band at $\sim 2700\ \mathrm{cm}^{-1}$, historically named G', since it is the second most prominent peak always observed in graphite samples [15]. The *G* peak is due to the doubly degenerate zone center E_{2g} mode [16]. On the contrary, the G' band has nothing to do with the *G* peak, but is the second order of zone-boundary phonons. Since zone-boundary phonons do not satisfy the Raman fundamental selection rule, they are not seen in first order Raman spectra of defect-free graphite [17]. Such phonons give rise to a peak at $\sim 1350\ \mathrm{cm}^{-1}$ in defected graphite, called *D* peak [16]. Thus, for clarity, we refer to

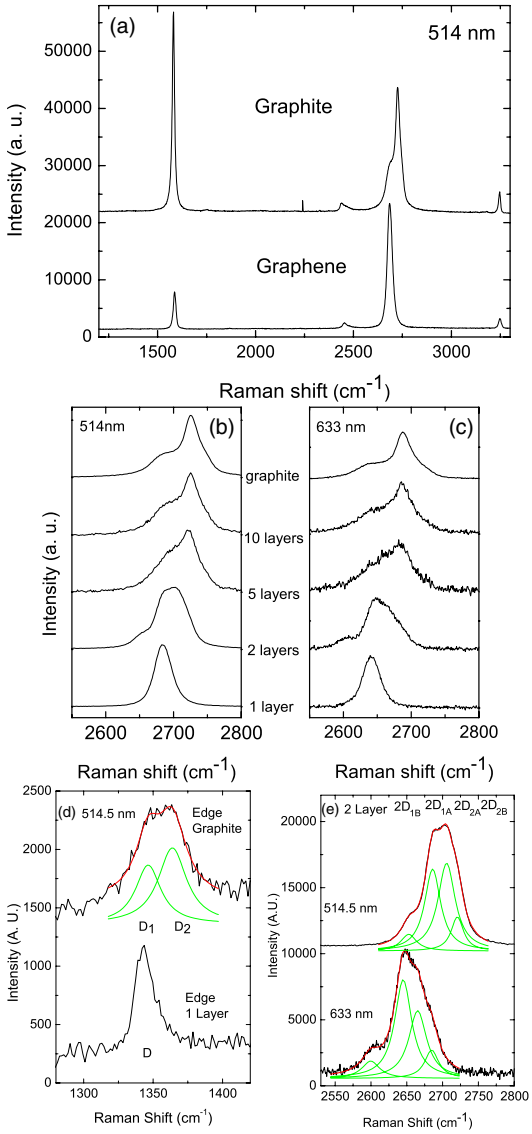

FIG. 2 (color online). (a) Comparison of Raman spectra at 514 nm for bulk graphite and graphene. They are scaled to have similar height of the 2*D* peak at $\sim 2700\ \mathrm{cm}^{-1}$. (b) Evolution of the spectra at 514 nm with the number of layers. (c) Evolution of the Raman spectra at 633 nm with the number of layers. (d) Comparison of the *D* band at 514 nm at the edge of bulk graphite and single layer graphene. The fit of the D_1 and D_2 components of the *D* band of bulk graphite is shown. (e) The four components of the 2*D* band in 2 layer graphene at 514 and 633 nm.

the G' peak as $2D$. Figure 2(a) shows that no D peak is observed in the center of graphene layers. This proves the absence of a significant number of defects. As expected, a D peak is only observed at the sample edge, Fig. 2(d). Figure 2(a) shows a significant change in shape and intensity of the $2D$ peak of graphene compared to bulk graphite. The $2D$ peak in bulk graphite consists of two components $2D_1$ and $2D_2$ [15,17], roughly $1/4$ and $1/2$ the height of the G peak, respectively. Here we measure a single, sharp $2D$ peak in graphene, roughly 4 times more intense than the G peak. Notably, the G peak intensity of single layer and bulk graphite is comparable [note that Fig. 2(a) is rescaled to show a similar $2D$ intensity] and the G position is 3–5 cm^{-1} higher than bulk graphite. This upshift is partially due to chemical doping. The change in shape of the $2D$ band is nicely confirmed in Fig. 2(d), which compares the D peak of the graphite edge with that of the graphene edge. The graphene D peak is a single sharp peak, while in graphite is a band consisting of two peaks D_1 and D_2 [15]. Figures 2(b) and 2(c) plot the evolution of the $2D$ band as a function of layers for 514.5 and 633 nm excitations. These immediately indicate that a bilayer has a much broader and up-shifted $2D$ band with respect to graphene. This band is also quite different from bulk graphite. It has 4 components, $2D_{1B}$, $2D_{1A}$, $2D_{2A}$, $2D_{2B}$; two of which, $2D_{1A}$ and $2D_{2A}$, have higher relative intensities than the other two, as indicated in Fig. 2(e). Figure 2(b) and 2(c) show that a further increase in layers leads to a significant decrease of the relative intensity of the lower frequency $2D_1$ peaks. For more than 5 layers the Raman spectrum becomes hardly distinguishable from that of bulk graphite. Thus Raman spectroscopy can clearly distinguish a single layer, from a bilayer from few (less than 5) layers. This also explains why previous experiments on nanographites, but not single or bilayer graphene, did not identify these features [18,19]. In particular, it was noted from early studies that turbostratic graphite (i.e., without AB stacking) has a single $2D$ peak [20]. However, its full width at half maximum (FWHM) is 50 cm^{-1} almost double that of the $2D$ peak of graphene and up-shifted of 20 cm^{-1}. Turbostratic graphite also often has a first order D peak [20]. Single wall carbon nanotubes (SWNTs) show a sharp $2D$ peak similar to that measured here for graphene [21]. The close similarity (in position and FWHM) of our measured graphene $2D$ peak and the $2D$ peak in SWNTs of 1–2 nm diam [22] implies that curvature effects are small for the $2D$ peak for SWNTs in this diameter range, the most commonly found in experiments. This questions the assumption that the $2D$ peak in SWNT should scale to the up-shifted average $2D$ peak position in bulk graphite for large diameters [22]. Thus the scaling law relating diameter and $2D$ peak position, often used to derive the inner diameter in double wall tubes [22,23], needs to be revisited. Despite the similarities, there are major differences between graphene and SWNT Raman spectra, which allow us to easily distinguish them. Indeed, confinement and curvature split the two degenerate modes of the G peak in SWNTs [21], resulting in G^+ and G^- peaks.

We now explain why graphene has a single $2D$ peak, and why this splits in four components in bilayer graphene. Several authors previously attempted to explain the double structure of the $2D$ peak in graphite [15,17–20,24], however they always neglected the evolution of the electronic bands with the number of layers, which is, on the contrary, the key fact. The $2D$ peak in graphene is due to two phonons with opposite momentum in the highest optical branch near the $\mathbf{K}$ (A_1' symmetry at $\mathbf{K}$) [16,25,26]. Figure 2 shows that this peak changes in position with varying excitation energy. This is due to a double resonance (DR) process, which links the phonon wave vectors to the electronic band structure [27].

Within DR, Raman scattering is a fourth order process involving four virtual transitions: (i) a laser induced excitation of an electron-hole pair [$a \rightarrow b$ vertical transition in Fig. 3(a)]; (ii) electron-phonon scattering with an exchanged momentum $\mathbf{q}$ close to $\mathbf{K}$ ($b \rightarrow c$); (iii) electron-phonon scattering with an exchanged momentum $-\mathbf{q}$ ($c \rightarrow b$); (iv) electron-hole recombination ($b \rightarrow a$). The DR condition is reached when the energy is conserved in these transitions. The resulting $2D$ Raman frequency is twice the frequency of the scattering phonon, with $\mathbf{q}$ determined by the DR condition. For simplicity, Figs. 3(a) and 3(b) neglect the phonon energy and do not show the equivalent processes for hole-phonon scattering. In addition, we only consider the dispersions along $\mathbf{\Gamma} - \mathbf{K} - \mathbf{M} - \mathbf{K}' - \mathbf{\Gamma}$. The transitions within this line correspond to the peaks in the phonon distribution fulfilling DR [19], once the trigonal warping is considered [28].

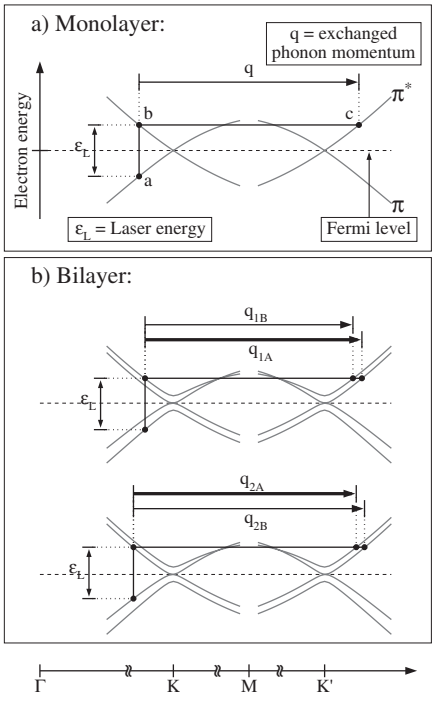

FIG. 3. DR for the 2D peak in (a) single layer and (b) bilayer.

TABLE I. Relative splitting of $2D$ components in bilayer graphene (in cm^{-1}). In each case, we show the shift with respect to the average frequency of the two main peaks. The four columns of the bilayer correspond to processes q_{1B}, q_{1A}, q_{2A}, q_{2B}, respectively. The theoretical values are obtained by multiplying the DR q vectors determined from the DFT electronic bands by $dw/dq = 645\ cm^{-1}$ Å. Here dw/dq is the ratio between the measured shift of the $2D$ peak frequency with the laser energy in graphene ($\sim 99\ cm^{-1}/eV$), and the corresponding variation of the DR $q \sim 2k$ computed from the DFT bands.

514.5 nm				
Experimental	−44	−10	+10	+25
Theory	−44	−11	+11	+41
633 nm				
Experimental	−55	−10	+10	+30
Theory	−44	−9	+9	+41

Consistent with the experimental observation of a single component for the $2D$ peak in single layer graphene, Figs. 3(a) and 3(b) only shows the phonon satisfying DR conditions with momentum $q > K$, along the $\mathbf{\Gamma} - \mathbf{K} - \mathbf{M}$ direction ($K < q < M$). The other two possible DR phonons, with $q < K$ and $q \sim K$, give a much smaller contribution to the Raman intensity. In fact, the $q < K$ phonon involves a smaller portion of the phase space because of the band-structure trigonal warping (see Figs. 3,4 of Ref. [28] and related discussion) and the $q \sim K$ phonon has a zero electron-phonon coupling for this transition, as discussed in Ref. [26] (see footnote 24, for $q \sim K$, $\theta'' = 0$) and Ref. [24]. This differs from the model of Ref. [24], which predicts 2 similar components for the D peak even in single layer, in disagreement with the experiments of Fig. 2.

We now examine the bilayer case. The observed 4 components of the $2D$ peak could in principle be attributed to two different mechanisms: the splitting of the phonon branches [15,17,20,29], or the spitting of the electronic bands [25]. To ascertain this we compute the phonon frequencies [26] for both single and bilayer graphene (stacked AB, as indicated by TEM), at the q corresponding to the DR condition for the 514 and 633 nm lasers. The splitting of the phonon branches is $<1.5\ cm^{-1}$, much smaller than the experimentally observed $2D$ splitting. Thus, this is solely due to electronic bands effects. In the bilayer, the interaction of the graphene planes causes the π and π^* bands to divide in four bands, with a different splitting for electrons and holes, Fig. 3(b). According to the density functional theory (DFT) dipole matrix elements, amongst the 4 possible optical transitions, the incident light couples more strongly the two transitions shown in Fig. 3(b). The two almost degenerate phonons in the highest optical branch couple all electron bands amongst them. The resulting four processes involve phonons with momenta q_{1B}, q_{1A}, q_{2A}, and q_{2B}, as shown in Fig. 3(b). The four corresponding processes for the holes, and those associated to the 2 less intense optical transitions [not shown in Fig. 3(b)], are associated to momenta almost identical to q_{1B}, q_{1A}, q_{2A}, q_{2B} and almost (within $\sim 0.2\ cm^{-1}$) identical Raman shifts. These wave vectors correspond to phonons with different frequencies, due to the strong phonon dispersion around **K** induced by the electron-phonon coupling [26]. They produce four different peaks in the Raman spectrum of bilayer graphene. Table I reports the expected splittings and shows that they compare very well with experiments.

In conclusion, graphene's electronic structure is uniquely captured in its Raman spectrum, that clearly evolves with the number of layers. Raman fingerprints for single-, bilayer, and few-layer graphene reflect changes in the electronic structure and electron-phonon interactions and allow unambiguous, high-throughput, nondestructive identification of graphene layers.

A. C. F. acknowledges funding from EPSRC No. GR/S97613, The Royal Society, and The Leverhulme Trust; C. C. acknowledges funding from the Oppenheimer Fund.

*Electronic address: acf26@eng.cam.ac.uk

[1] K. S. Novoselov *et al.*, Proc. Natl. Acad. Sci. U.S.A. **102**, 10 451 (2005).
[2] K. S. Novoselov *et al.*, Nature (London) **438**, 197 (2005).
[3] Y. Zhang *et al.*, Nature (London) **438**, 201 (2005).
[4] K. S. Novoselov *et al.*, Science **306**, 666 (2004).
[5] K. S. Novoselov *et al.*, Nature Phys. **2**, 177 (2006).
[6] Y. Zhang *et al.*, Appl. Phys. Lett. **86**, 073104 (2005).
[7] N. M. Peres *et al.*, Phys. Rev. B **73**, 125411 (2006).
[8] C. Berger *et al.*, J. Phys. Chem. B **108**, 19 912 (2004).
[9] K. Wakabayashi, Phys. Rev. B **64**, 125428 (2001).
[10] K. Nakada *et al.*, Phys. Rev. B **54**, 17 954 (1996).
[11] J. Scott Bunch *et al.*, Nano Lett. **5**, 287 (2005).
[12] P. R. Wallace, Phys. Rev. **71**, 622 (1947).
[13] L. M. Viculis, J. J. Mack, and R. B. Kaner, Science **299**, 1361 (2003).
[14] J. C. Meyer *et al.*, Ultramicroscopy **106**, 176 (2006); Science **309**, 1539 (2005).
[15] R. P. Vidano *et al.*, Solid State Commun. **39**, 341 (1981).
[16] F. Tuinstra and J. Koenig, J. Chem. Phys. **53**, 1126 (1970).
[17] R. J. Nemanich and S. A. Solin, Phys. Rev. B **20**, 392 (1979).
[18] L. G. Cancado *et al.*, Phys. Rev. Lett. **93**, 047403 (2004).
[19] L. G. Cancado *et al.*, Phys. Rev. B **66**, 035415 (2002).
[20] P. Lespade *et al.*, Carbon **22**, 375 (1984).
[21] A. Jorio *et al.*, Phys. Rev. B **66**, 115411 (2002).
[22] A. G. Souza Filho *et al.*, Phys. Rev. B **67**, 035427 (2003).
[23] R. Pfeiffer *et al.*, Phys. Rev. B **71**, 155409 (2005).
[24] J. Maultzsch, S. Reich, and C. Thomsen, Phys. Rev. B **70**, 155403 (2004).
[25] A. C. Ferrari and J. Robertson, Phys. Rev. B **61**, 14 095 (2000).
[26] S. Piscanec *et al.*, Phys. Rev. Lett. **93**, 185503 (2004).
[27] C. Thomsen and S. Reich, Phys. Rev. Lett. **85**, 5214 (2000).
[28] J. Kurti *et al.*, Phys. Rev. B **65**, 165433 (2002).
[29] A. C. Ferrari and J. Robertson, Phil. Trans. R. Soc. A **362**, 2267 (2004).